Earth and Planetary Science Letters 559 (2021) 116786

Contents lists available at ScienceDirect

Earth and Planetary Science Letters

www.elsevier.com/locate/epsl

Modeling long-term delta dynamics reveals persistent geometric river avulsion locations

Katherine M. Ratliff [a,*,1], Eric W.H. Hutton [b], A. Brad Murray [a]

[a] Division of Earth & Ocean Sciences, Nicholas School of the Environment, Duke University, Box 90230, Durham, NC 27708-0230, USA
[b] Community Surface Dynamics Modeling System, University of Colorado, Campus Box 450, Boulder, CO 80309-0450, USA

ARTICLE INFO

Article history:
Received 17 July 2020
Received in revised form 18 December 2020
Accepted 23 January 2021
Available online 1 February 2021
Editor: J.-P. Avouac

Keywords:
river delta
river avulsion
avulsion node
delta morphodynamics

ABSTRACT

River deltas grow through repeated stacking of sedimentary lobes, the location and size of which are determined by channel avulsions (relatively sudden changes in river course). We use a model coupling fluvial and coastal processes to explore avulsion dynamics under a range of wave energies and sea-level-rise rates and find that the primary control on avulsion location and delta lobe size in our model is the critical superelevation ratio (*SER*), the amount of channel aggradation relative to the surrounding floodplain that is required to trigger an avulsion. The preferred avulsion location arises because of geometric constraints – a preferential avulsion node occurs at the break in floodplain slope that develops as the river progrades and/or sea level rises. This concavity develops in our model because the river profile aggrades and erodes via linear diffusion, whereas the diffusion of the floodplain topography is limited to episodic crevasse splays. These results are in contrast to recent modeling work, which was motivated by laboratory experiments and assumes a union between river channel and floodplain aggradation rates, and where avulsion nodes are driven by backwater hydrodynamics. The preferred avulsion length in our model scales well with laboratory, field, and model results without including hydrodynamic backwater effects. This work suggests an alternative mechanism to explain avulsion locations on deltas where floodplain topography aggrades and/or diffuses more slowly than the river channel profile, and it points to the need to elucidate river channel and floodplain connectivity over large space and time scales, and how the connectivity varies from one type of delta to another.

Published by Elsevier B.V.

1. Introduction

More than half a billion people live on or near deltas, as their low-lying, fertile landscapes have long been ideal locations for human settlement (J. P. M. Syvitski et al., 2009). These landscapes have become increasingly vulnerable to submergence as sea-level rise, accelerated subsidence, and decreased upstream sediment supply all lower deltaic elevations relative to sea level (Blum and Roberts, 2009; Tessler et al., 2015). Rivers typically deliver sediment to one part of a delta at a time, successively building distinct lobes, and channel avulsion dynamics control both the location and size of delta lobes. These avulsions, which occur when the river changes its course, are often associated with channel superelevation, which is a measure of the water surface elevation in the channel at bankfull discharge relative to the far-field floodplain (i.e., beyond levee relief) and is correlated with channel levee relief (Hajek and Wolinsky, 2012; Mohrig et al., 2000). Because avulsions pose hazards to inhabitants and infrastructure (Sinha, 2009), a better understanding of natural avulsion dynamics and where an avulsion is most likely to occur facilitates improved and more sustainable management practices (Paola et al., 2011).

Field, laboratory, and modeling studies have indicated that avulsion nodes on deltas tend to occur at a distance from the river mouth that scales with the "backwater zone", the lowermost portion of the river near the mouth, where flow is affected by the presence of the receiving lake or ocean basin (Chadwick et al., 2019; Chatanantavet et al., 2012; Ganti et al., 2016a, 2016b; Jerolmack, 2009). The length of the backwater zone is approximated by $L_B \approx D/S$, where D is a characteristic flow depth (here, the bankfull channel depth) and S is the riverbed slope (Paola, 2000). Recent work (Chadwick et al., 2019; Chatanantavet et al., 2012; Ganti et al., 2014, 2016b), motivated in part by field observations (Nittrouer et al., 2011, 2012), credits hydrodynamic backwater effects as the primary driver of avulsion location; repeated alternations between flooding events and lower flows create a peak in

* Corresponding author.
E-mail addresses: ratliff.katherine@epa.gov (K.M. Ratliff), eric.hutton@colorado.edu (E.W.H. Hutton), abmurray@duke.edu (A.B. Murray).
[1] Present address: U.S. Environmental Protection Agency, Office of Research and Development, 109 TW Alexander Drive, Research Triangle Park, NC 27711, USA.

https://doi.org/10.1016/j.epsl.2021.116786
0012-821X/Published by Elsevier B.V.

net channel sedimentation at a location that scales with L_B, driving avulsions at this location of maximum deposition (and channel superelevation).

Here, we show that an alternative mechanism could explain the observed scaling for some deltas—a mechanism that doesn't involve hydrodynamic backwater effects, but instead arises from morphodynamic processes that give rise to differences in the geometry of the longitudinal river profile relative to that of the surrounding floodplain as the delta evolves over time. If fluvial sediment transport processes diffuse the longitudinal river profile more rapidly than floodplain deposition during floods smooths floodplain topography, then either channel progradation or base level rise will drive in-channel aggradation that causes the river profile to become super-elevated most quickly at a distance that scales with the backwater length. This geometric explanation, which is supported by preliminary comparisons to some large natural deltas, arises from the results of simple numerical modeling experiments. In order to most clearly understand how geometrical constraints on avulsion locations can arise, we describe here, step by step, how the delta landscape evolves from the dynamics represented in the model. This preferred avulsion location persists over a range of wave influences and sea-level rise rates without explicitly including hydrodynamic backwater effects or varying flows.

2. Methods

2.1. Coupled model description

In the River Avulsion and Floodplain Evolution Model (RAFEM), cell widths are greater than channel widths, such that the channel belt is contained within a single cell, and within-channel processes are not resolved. Natural levees, although not explicitly resolved, exist adjacent to the river channel within the river cells (Aalto et al., 2003; Pizzuto, 1987; Walling and He, 1998), and levee elevation is maintained at one bankfull channel depth above the river bed elevation (Hoyal and Sheets, 2009; Jerolmack and Paola, 2007). Herein, 'floodplain elevation' refers to the elevations in the adjacent floodplain cells (not the elevation of the natural levee topography). The river course is determined using a steepest-descent algorithm (Jerolmack and Paola, 2007) that compares the elevations of the three downstream and two cross-stream cells (i.e., no upstream flow is permitted). Erosion and deposition along the river channel are modeled as a linear diffusive process (Paola, 2000), and the bed elevation at the river mouth is held at a constant channel depth below sea level, such that either shoreline progradation or base-level rise will cause a diffusive wave of aggradation to migrate upstream.

An avulsion is triggered when a river cell meets or exceeds the critical superelevation ratio [*SER* (Table S1), the elevation difference between the levee elevation and the minimum elevation of the adjacent (i.e., two cross-stream) floodplain cells, normalized by bankfull channel depth (Mohrig et al., 2000; Ratliff et al., 2018)], and a new steepest-descent path to sea level is determined. If the new path is shorter than the prior river course, the avulsion occurs (Ganti et al., 2016b; Slingerland and Smith, 2004). However, if the new path is longer than the previously-existing one, the avulsion does not occur, representing an avulsion that would not be successful along a shallower channel gradient with a decreased sediment transport capacity (Hoyal and Sheets, 2009; Slingerland and Smith, 2004). Instead, a crevasse splay is deposited (Shen et al., 2015; van Toorenenburg et al., 2016) at the failed avulsion branch, adjacent to the river channel. The crevasse splay is deposited in the first failed channel cell and the adjacent floodplain cells, with the deposition rate tied to the in-channel aggradation rate upstream of the splay in the river channel (Ratliff et al., 2018). In these experiments, we seed an initial downstream-sloping landscape with random variability, and the parameter values are consistent with Ratliff et al. (2018) [see Ratliff et al. (2018) for a more complete description of RAFEM].

The bedload sediment flux (i.e., sand) from the RAFEM river mouth is retained in the shoreline and distributed alongshore using the Coastline Evolution Model [CEM (A. Ashton et al., 2001; A. D. Ashton and Murray, 2006)], a one-line model in which gradients in wave-driven alongshore sediment transport, Q_s, cause erosion and accretion of the shoreline and nearshore seabed. Erosion and accretion extend offshore to the shoreface depth, D_{sf}, below which wave-driven sediment transport becomes negligible. Assuming an approximately constant long-term shoreface profile geometry and conservation of nearshore sand leads to:

$$\frac{d\eta}{dt} = -\frac{1}{D_{sf}}\frac{dQ_s}{dx} \tag{1}$$

where η is shoreline position, t is time, and x is the alongshore direction.

In CEM, offshore wave-approach angles change every model day, and coastline-shape evolution depends on the mix of influences from different angles [the 'wave climate' (A. D. Ashton and Murray, 2006)]. In experiments reported here, the net effect of the wave climate is to diffusively smooth the plan view coastline shape, with a symmetric mix of influences from the left and right. The wave height, which represents an effective average value (A. D. Ashton and Murray, 2006), remains constant over each experiment. If part of the delta lobe blocks a shoreline cell from the current offshore wave direction, then no sediment transport occurs in this "wave-shadowed zone", which approximates the effect of decreased wave energy within and adjacent to this region (from wave refraction and diffraction).

RAFEM and CEM are coupled using the Community Surface Dynamics (CSDMS) Basic Model Interface (Peckham et al., 2013), and model sensitivity analyses were conducted using the Dakota toolkit (Adams et al., 2014). Both RAFEM and CEM are available as part of the CSDMS model repository (https://csdms.colorado.edu) and can be downloaded and coupled using *pymt*, a Python toolkit for running and coupling Earth surface models (https://pymt.readthedocs.io). The parameter values used here are consistent with the values used in Ratliff et al. (2018).

2.2. Floodplain elevation profiles

Results from the coupled RAFEM-CEM model are also compared to natural systems. Using ArcMap 10.6, a 15 km buffer was generated around global river centerlines (1:50m 'medium' scale data, downloaded from NaturalEarthData.com on 16 August 2018) and exported as a .kmz file for viewing in GoogleEarth. The 15 km buffer lines following the right bank (looking downstream) of the Mississippi River and the left bank (looking downstream) of the Brahmaputra River were traced, and elevation data along these profiles was extracted using the GEOCONTEXT-PROFILER (http://www.geocontext.org/publ/2010/04/profiler/en/). The lower 1000 km of these profiles was then smoothed using a Savitzky-Golay filter (window length = 5, polynomial order = 3). Locations of the avulsion nodes were determined using visual comparison of the floodplain profiles and the river channels in GoogleEarth.

3. Results: modeled delta landscape evolution

This model framework hinges on how the river profile evolves, representing the large-scale, long-term effects of longitudinal sediment flux gradients as diffusional processes (Paola, 2000). As an initial condition, we start from a pre-existing (planar) landscape, representing previous river deposits, intersecting sea level

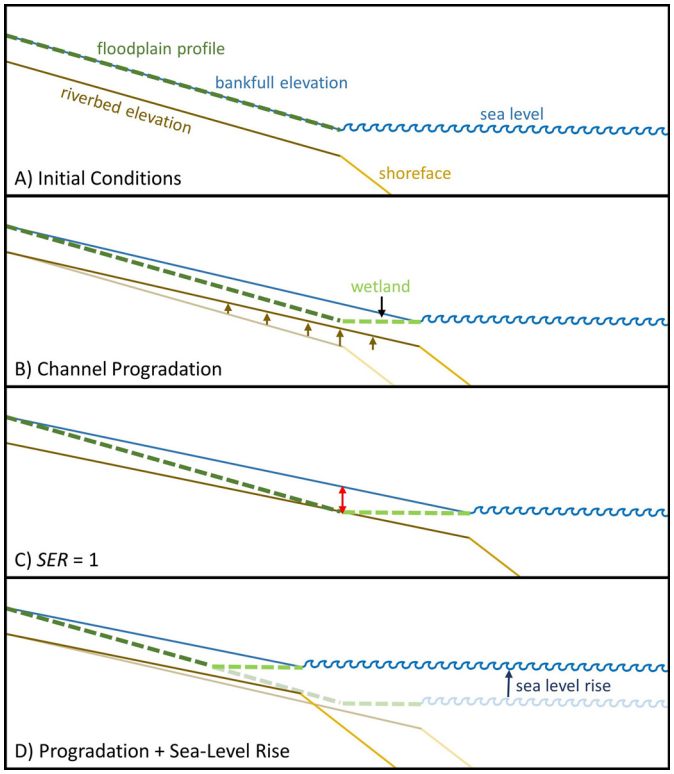

Fig. 1. Illustration of profile view of riverbed and surrounding floodplain geometry over time. A) Initial model conditions with dashed floodplain profile exactly overlaying bankfull water surface elevation profile. B) Profiles after channel progradation, where brown arrows represent riverbed aggradation relative to the previous profile (faded lines). Kink in floodplain profile develops where wetlands that form as the delta progrades intersect the sloping floodplain profile. C) Critical *SER* met at the red arrow; bankfull water surface elevation is a channel depth above the floodplain, and the riverbed elevation has reached that of the floodplain at the kink (and has reached the elevation of sea level). D) An example profile with sea-level rise and progradation. For reference, faded lines represent profiles without sea-level rise imposed. Floodplain profile kink migrates upslope as wetlands aggrade at the same rate that sea level rises. Sea-level rise also induces shoreline erosion assuming a quasi-equilibrium generalized Bruun Rule (Ratliff et al., 2018), causing a tendency for the river mouth to retrograde as sea level rises (while fluvial sediment deposition tends to cause progradation). (For interpretation of the colors in the figure(s), the reader is referred to the web version of this article.)

(Fig. 1A). As the river deposits sediment at the shoreline, the river mouth progrades seaward, and longitudinal diffusion smooths the river profile, such that the riverbed aggrades as a diffusive wave of riverbed deposition propagates upstream of the river mouth (Fig. 1B). We assume that natural levees form adjacent to the river channel (Aalto et al., 2003; Pizzuto, 1987; Walling and He, 1998) and that their aggradation rate is fully coupled to that of the river bed. However, we do not assume that the landscape farther away from the river channel aggrades at rates that are tightly coupled to that of the riverbed. Floodplain elevations do increase as crevasse splays occur (Shen et al., 2015; van Toorenenburg et al., 2016), but the resulting deposition rates are not sufficient in our model experiments for the distal floodplain to aggrade at the same rate as the river channel. More significantly, we represent wetland development in the area adjacent to the river behind the prograding shoreline by imposing a minimum elevation in all areas landward of the prograding shoreline that is slightly above sea level.

Therefore, as the river mouth progrades, a horizontal portion of the delta floodplain profile develops (Fig. 1B). If sea level is held constant, the elevations of the sloping and horizontal portions of the distal floodplain remain approximately constant through time, while the river profile continues to lengthen, diffuse, and aggrade (Fig. 1C). The superelevation of the riverbed, relative to the floodplains that are above sea level, develops most rapidly in the zone surrounding the break in slope of the floodplain profile. If the threshold *SER* required to trigger an avulsion is 1, then the avulsion cannot occur until the horizontal delta plain widens and progrades far enough for the riverbed elevation to reach that of sea level. So, the model dynamics of the river profile evolution relative to the floodplain profile evolution lead to avulsions that occur at a distance from the river mouth that scales with L_B.

Although the avulsion location is always associated with the floodplain slope break, the distance from the river mouth to an avulsion location [the avulsion length (L_A)] depends on the diffusivity of the river profile and on the threshold *SER*. Studies of avulsions in the field (Mohrig et al., 2000) indicate that avulsions generally occur at $SER = 0.5$-1 (Hajek and Wolinsky, 2012), but this value is significantly less for some systems [e.g., Mississippi River, <0.1 (Törnqvist and Bridge, 2002)]. The critical *SER* in prototypical channels can be affected by many factors, including levee grain size, cohesiveness, and vegetation. Here, we use a critical *SER* of either 0.5 or 1 to explore how avulsion dynamics depend on this parameter. If the riverbed elevation must aggrade to that of the surrounding floodplain elevation ($SER = 1$, Fig. 2A), then L_A is between 1.5 and 2 L_B over several orders of magnitude in sea level rise rates ($SLRR^*$, Table S1). If $SER = 0.5$ (Fig. 2B), L_A is close to L_B. This scaling with *SER* arises because a higher *SER* requires more in-channel aggradation (and associated progradation) to trigger an avulsion, and it is similar to recent modeling results of avulsion processes with variable flow regimes (Chadwick et al., 2019) and flume experiments (Ganti et al., 2016b). Because L_A controls the extent to which the delta progrades into the basin (Ganti et al., 2016a), our results also suggest that delta size scales with the critical *SER*.

The model framework also involves the plan view evolution of the delta (Fig. 3), which depends on the rate of fluvial sediment delivery relative to the rate of wave-driven coastline smoothing (see Section 2.1). Smaller wave heights lead to more rugose shorelines, as sediment is delivered to the coast more rapidly than waves can spread it alongshore ['river dominated', Fig. 3A; Nienhuis et al. (2015); Ratliff et al. (2018)]. With increasing wave influence, alongshore sediment transport redistributes the river sand more rapidly, forming more cuspate to nearly flat, smooth shorelines ('wave dominated', Fig. 3C). Experiments using a wide range of ratios between sediment delivery and wave-driven sediment redistribution, with relatively low wave heights (WH^*, Table S1) for river-dominated delta types (Fig. 3A) to relatively high wave influence for wave-dominated deltas (Fig. 3C), show that L_A is not sensitive to the plan view dynamics (Fig. 2). The degree of wave influence does, however, impact how rapidly avulsions occur (Ratliff et al., 2018).

In model experiments featuring rising sea level, the bed elevation at the river mouth rises along with sea level, causing an increased diffusion and aggradation of the river profile upstream. In addition, we assume that the elevation of the horizontal portion of the delta plain, which approximates marshes that aggrade at the rate of sea-level rise [even at high sea-level rise rates, given sufficient sediment supply (Kirwan et al., 2016; Ratliff et al., 2015)], also rises at the same rate. This causes the break in slope in the floodplain profile to migrate up slope (Fig. 1D); however, the geometric relationship of the river and floodplain profiles that drives avulsions at the location of maximum floodplain curvature is not qualitatively changed relative to the no sea-level rise condition, and avulsions still occur at the migrating break in floodplain slope.

Natural and laboratory delta floodplains are unlikely to exhibit a break in floodplain slope that is as pronounced as the one that arises from our model assumptions (Fig. 1). Floodplain deposition (including crevasse splay deposition) will tend to diffuse the landscape. In addition, nonuniform subsidence will influence topo-

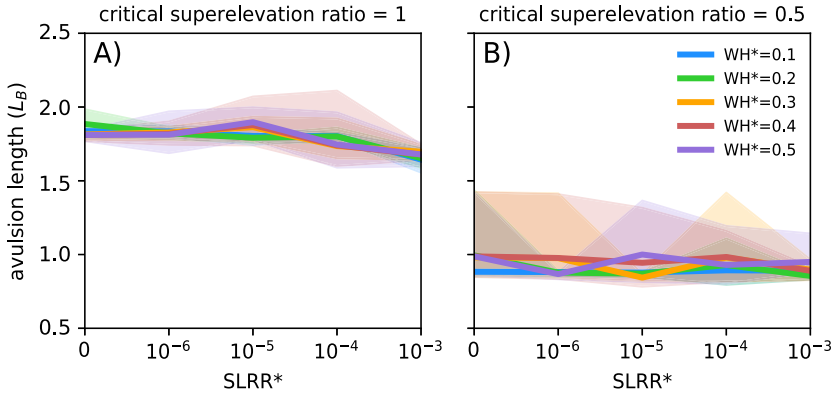

Fig. 2. Avulsion length (L_A, measured in number of geometric backwater lengths, L_B) for critical $SER = 1$ (A) and 0.5 (B) for a range of wave influences (WH^*) and range of $SLRR^*$. Envelopes represent range of values from five sets of numerical experiments, and lines represent average values. L_A is slightly less than one backwater length L_B for $SER = 0.5$ and between 1.5 and 2 L_B for $SER = 1$. Leftmost point on $SLRR^*$ represents experiments with no sea level rise (i.e., the axis is not in true log scale).

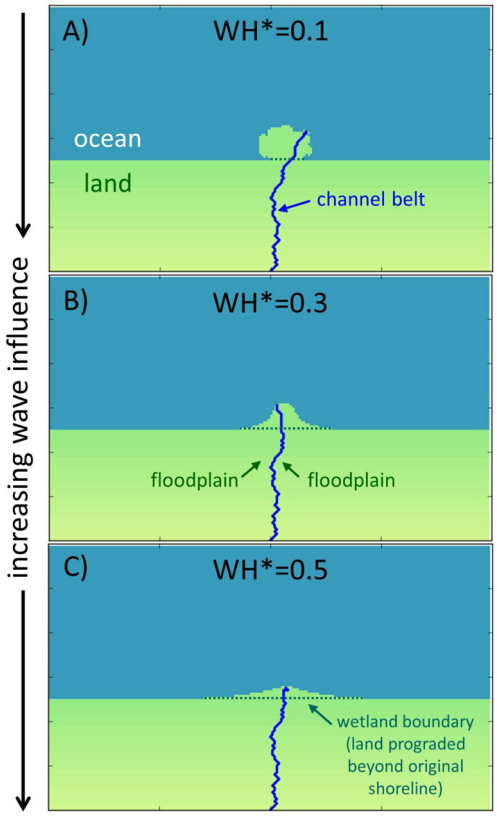

Fig. 3. Planview morphology of deltas in a symmetric, diffusive wave climate with increasing wave influence from top (A, river-dominated delta) to bottom (C, wave-dominated delta), where WH* is wave height nondimensionalized by channel depth, D. Critical $SER = 1$. Blue line represents the river cells, and the land formed behind the shoreline of the prograding delta (seaward of the dashed line) represents the wetland area.

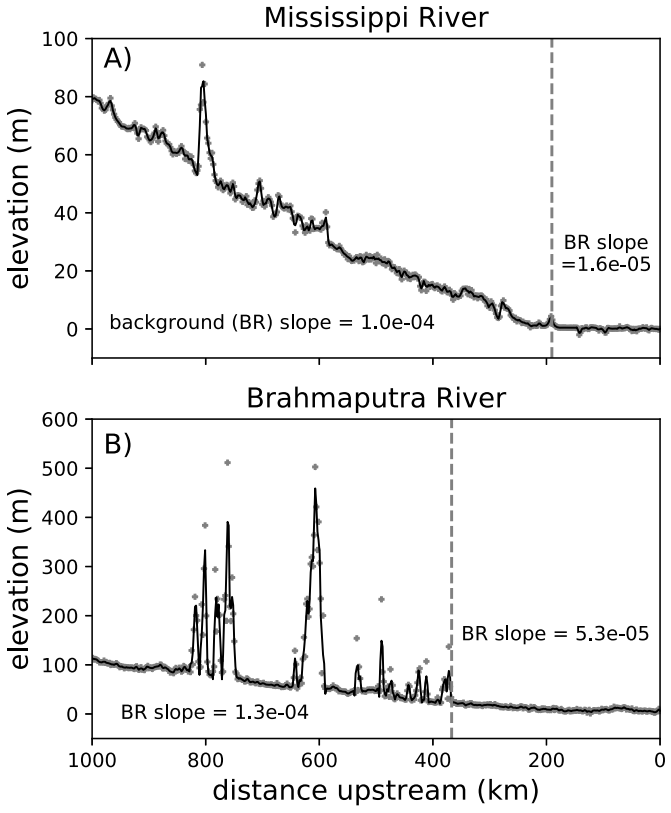

Fig. 4. Distal floodplain elevation profiles for (A) the Mississippi River and (B) the Brahmaputra River. Distance upstream as noted in the profiles is from the Head of Passes for the Mississippi River and from the river mouth of Meghna River for the Brahmaputra River. Elevation data was extracted along 15 km buffer following the river centerlines (see Section 2.2). Dots represent elevation datapoints, and solid black lines represent the smoothed profiles using a Savitzky-Golay filter. Dashed vertical lines indicate the location of the most recent major channel avulsion along each river, and the background slope (BR, calculated using the elevations at the upstream and downstream ends of each section up and downstream of the avulsion) for each floodplain profile segment corresponds to its location above or below the avulsion node.

graphic lows in floodplains relative to an aggrading river profile. However, we find that the tendency for the floodplains of depositional river lobes to have vanishingly small slopes near the river mouth is present on natural deltas (Fig. 4). The distal floodplain elevation profiles for both the Mississippi (Fig. 4A) and the Brahmaputra (Fig. 4B) rivers show a distinct slope transition, similar to the evolution of our model geometry and results. The approximate locations of the most recent major avulsions on both rivers – the Lafourche avulsion site on the Mississippi (Aslan et al., 2005; Chamberlain et al., 2018), and the Brahmaputra avulsion node on the upper delta plain of the Bengal Basin (Pickering et al., 2014; Sincavage et al., 2018) – are also plotted. The 'background' slopes of the floodplains upstream and downstream of the avulsion node show a significant transition. For the Mississippi, the upstream slope is >6 times the delta plain slope, and the upland slope of the Brahmaputra floodplain is approximately 2.5 times greater than the lobe floodplain slope. The slope break occurs within the backwater zone of the Mississippi River (Aslan et al., 2005; Chamberlain et al., 2018; Chatanantavet et al., 2012), but the slope break identified in Fig. 4B is upstream of

the backwater zone on the Brahmaputra River (Pickering et al., 2014; Sincavage et al., 2018; Wilson and Goodbred, 2015). For both the Mississippi and Brahmaputra Rivers, the most recent major avulsions occurred at the break in floodplain slope, similar to the floodplain geometry adjacent the preferred avulsion node in our model. Note that the river channel profiles are not plotted alongside floodplain profiles in Fig. 4 because the sinuosity of the channels and its impact on the distal floodplain profile extracted as described in Section 2.2 causes a mismatch between the floodplain and channel profile lengths, making a direct comparison between the two profiles (including both sides of the floodplain profiles) over long portions of the river courses difficult. Floodplain profiles from the Yellow River and the Mekong River also exhibit slope transitions (Fig. S1). The profiles and avulsion histories presented here are not intended to represent a comprehensive comparison for deltas across the globe, but rather to demonstrate that this slope transition can, in fact, be present on field-scale deltas. These initial comparisons highlight the need for future research.

4. Discussion and conclusions

The break in slope that develops in the distal floodplain in our model experiments is an exaggeration relative to natural systems. However, the aggradation of the river profile drives flooding, which in turn drives floodplain deposition. So, deposition on the floodplain, at some distance from the river, likely lags behind aggradation of the riverbed. The magnitude of this lag probably varies in different systems and settings, but as long as the distal floodplain deposition rates are lower than that of the riverbed, then the effective rate of longitudinal diffusion of the floodplain profile is lower than that of the river profile. Thus, for prograding rivers or those experiencing base-level rise, some zone along the fluvial profile will exist in which the floodplain profile has a higher curvature than the river profile. The break in slope in our model experiments represents the zone of maximum curvature of a floodplain profile that results from the interplay between previous river deposits and sea level. Preliminary comparisons to large deltas (Fig. 4) suggest that these dynamics are relevant on at least some natural deltas.

Recent numerical modeling work including backwater hydrodynamics has shown using previously developed numerical models that the geometrically-driven avulsion effect is a model artifact that cannot persist beyond a few avulsion cycles (Chadwick et al., 2019; Moodie et al., 2019). The differences between our results and the previous modeling results arise from fundamentally different assumptions about floodplain deposition. The floodplain deposition in the models from Chadwick et al. (2019) and Moodie et al. (2019) is directly coupled to river aggradation, such that the profiles of the rivers and the floodplains evolve towards the same shape. In Chadwick et al. (2019), the river course and avulsions are restricted to a set number of delta lobes, and just before an avulsion, the profiles of previous/unoccupied lobes are less prograded/aggraded than the present lobe. But, since the two profiles have the same shape, the geometric effect that arises in our model, which strongly favors avulsions at distances that scale with L_B over many avulsion cycles, cannot occur in their modeling framework, and avulsions can occur farther upstream under constant-discharge scenarios.

In the models where localized avulsions that scale with the backwater length only persist if variable discharges are included, the assumption that the surrounding floodplain gains elevation at exactly the same rate as the riverbed during progradation represents an endmember. In contrast, the corresponding assumption in our model represents the opposite endmember: that floodplain deposition can lag significantly behind the river aggradation that drives it. Under these conditions, as the delta lobe progrades, a transition in slope will naturally arise between the recently created land near the river mouth (land that would only be slightly above sea level) and the older landscape farther upstream that has experienced floodplain deposition for a longer period. Although the slope transition that arises in our model results is more abrupt than is likely under natural conditions, the fundamental dynamics leading to backwater-scaled avulsions only depend on the existence of some degree of slope transition – a zone of maximum curvature – in the floodplain profile. We believe that the assumptions underlying the dynamics in our model, including the development of the floodplain profile, are just as reasonable as the assumptions made in the models that have been motivated by laboratory experiments, where floodplain deposition is modeled as remaining in lockstep with channel aggradation. In reality, floodplain deposition processes on natural deltas must lie somewhere in between these endmember model assumptions (and likely vary among deltas of different types).

Currently, information is lacking about floodplain deposition processes, particularly over large spatial scales and at locations farther from the active channel belt. Moreover, floodplain deposition patterns, relative to channel aggradation, differ widely among different settings [e.g., confined valley vs. open delta plain, fan delta with mobile channels vs. vegetated deltas with stable channels; J. P. M. Syvitski et al. (2012)]. The fact that our model and the previous models utilize such contrasting assumptions illuminates needs for future research, both observational and modeling. Future work with the RAFEM-CEM coupled model will focus on varying how tightly coupled floodplain deposition is to riverbed aggradation rates, and how far laterally this coupling extends. We hypothesize that in the limit of complete coupling over very large lateral distances, the results of our model will converge with others (Chadwick et al., 2019; Moodie et al., 2019), although some differences may persist related to how these models treat the lateral/alongshore direction.

The relationship between L_A and *SER* in laboratory experiments (Chatanantavet et al., 2012; Ganti et al., 2014, 2016b) is consistent with the relationship in our model. However, the floodplain-deposition assumptions in models featuring backwater hydrodynamics (Chadwick et al., 2019; Moodie et al., 2019), which were motivated by conditions observed in laboratory experiments (Ganti et al., 2016a, 2016b), likely represent laboratory deltas better than the floodplain-deposition assumptions in our model. Given that channels are highly mobile and that flow that is not thoroughly confined in channels (Ganti et al., 2016a, 2016b), floodplain deposition likely keeps pace with the aggrading river profile more effectively than it does in our model. Because these laboratory dynamics are more in line with the model assumptions from Chadwick et al. (2019) and Moodie et al. (2019), the hydrodynamic backwater explanation may well be more relevant in the laboratory case than the geometrical explanation. However, many natural rivers do not exhibit the same degree of floodplain connectivity, and their channels in many settings are more confined (i.e., vegetated) and less mobile than in laboratory studies. This is particularly true where anthropogenic modifications of river courses have minimized or even prevented overbank sedimentation (J. P. Syvitski and Kettner, 2011). These 'hard' engineering controls cause channels to become super-elevated more rapidly, especially where subsidence rates are high (Jankowski et al., 2017), which can cause channels to be more prone to avulsions.

In both geometrically-constrained and variable-flow-driven avulsions, the avulsion location and delta size scale with the critical *SER*. A better understanding of what drives this critical value in natural rivers (where measured values have spread more than an order of magnitude) will improve predictions of where avulsions are most likely to occur. Further, more research is needed to constrain floodplain deposition rates over large space and time scales and to elucidate how tightly coupled these deposition rates are

to river channel aggradation rates in different systems. These insights will also be useful for planning targeted sediment diversions along river channels, which aim to restore deteriorating wetlands and mitigate land loss (Elsey-Quirk et al., 2019). An added benefit of these managed diversions may be reducing the risk of channel avulsions through increasing floodplain elevations (and decreasing channel superelevation) in locations where a river may be more prone to avulsion without the construction of additional hard engineering works.

CRediT authorship contribution statement

Katherine M. Ratliff: Conceptualization, Investigation, Methodology, Software, Visualization, Writing – original draft. **Eric W.H. Hutton:** Methodology, Resources, Software. **A. Brad Murray:** Conceptualization, Supervision, Writing – review & editing.

Declaration of competing interest

The authors declare that they have no known competing financial interests or personal relationships that could have appeared to influence the work reported in this paper.

Acknowledgements

CSDMS gratefully acknowledges major funding through a cooperative agreement with the National Science Foundation, EAR 0621695. K. Ratliff and A.B. Murray acknowledge support from NSF EAR 13-24114 and K. Ratliff was also supported by NSF GRFP DGF1106401. We thank Mike Lamb, Andrew Moodie, and Austin Chadwick for insightful discussions about this work. We acknowledge computing time on the CU-CSDMS High-Performance Computing Cluster.

Appendix A. Supplementary material

Supplementary material related to this article can be found online at https://doi.org/10.1016/j.epsl.2021.116786.

References

Aalto, R., Maurice-Bourgoin, L., Dunne, T., Montgomery, D.R., Nittrouer, C.A., Guyot, J.-L., 2003. Episodic sediment accumulation on Amazonian flood plains influenced by El Nino/Southern Oscillation. Nature 425 (6957), 493–497. https://doi.org/10.1038/nature02002.

Adams, B.M., Bauman, L., Bohnhoff, W., Dalbey, K., Ebeida, M., Eddy, J., et al., 2014. Dakota, a Multilevel Parallel Object-Oriented Framework for Design Optimization, Parameter Estimation, Uncertainty Quantification, and Sensitivity Analysis: Version 6.0 Users Manual. Sandia National Laboratories.

Ashton, A., Murray, A.B., Arnoult, O., 2001. Formation of coastline features by large-scale instabilities induced by high-angle waves. Nature 414 (6861), 296–300.

Ashton, A.D., Murray, A.B., 2006. High-angle wave instability and emergent shoreline shapes: 1. Modeling of sand waves, flying spits, and capes. J. Geophys. Res., Earth Surf. 111 (F4). https://doi.org/10.1029/2005JF000422.

Aslan, A., Autin, W.J., Blum, M.D., 2005. Causes of river avulsion: insights from the late Holocene avulsion history of the Mississippi River, USA. J. Sediment. Res. 75 (4), 650–664.

Blum, M.D., Roberts, H.H., 2009. Drowning of the Mississippi Delta due to insufficient sediment supply and global sea-level rise. Nat. Geosci. 2 (7), 488–491. https://doi.org/10.1038/NGEO553.

Chadwick, A.J., Lamb, M.P., Moodie, A.J., Parker, G., Nittrouer, J.A., 2019. Origin of a preferential avulsion node on lowland river deltas. Geophys. Res. Lett. https://doi.org/10.1029/2019gl082491.

Chamberlain, E.L., Törnqvist, T.E., Shen, Z., Mauz, B., Wallinga, J., 2018. Anatomy of Mississippi Delta growth and its implications for coastal restoration. Sci. Adv. 4 (4), eaar4740. https://doi.org/10.1126/sciadv.aar4740.

Chatanantavet, P., Lamb, M.P., Nittrouer, J.A., 2012. Backwater controls of avulsion location on deltas. Geophys. Res. Lett. 39 (1). https://doi.org/10.1029/2011GL050197.

Elsey-Quirk, T., Graham, S.A., Mendelssohn, I.A., Snedden, G., Day, J.W., Shaffer, G., et al., 2019. Mississippi River sediment diversions and coastal wetland sustainability: synthesis of responses to freshwater, sediment, and nutrient inputs. Estuar. Coast. Shelf Sci. https://doi.org/10.1016/j.ecss.2019.03.002.

Ganti, V., Chadwick, A.J., Hassenruck-Gudipati, H.J., Fuller, B.M., Lamb, M.P., 2016a. Experimental river delta size set by multiple floods and backwater hydrodynamics. Sci. Adv. 2 (5), e1501768. https://doi.org/10.1126/sciadv.1501768.

Ganti, V., Chadwick, A.J., Hassenruck-Gudipati, H.J., Lamb, M.P., 2016b. Avulsion cycles and their stratigraphic signature on an experimental backwater-controlled delta. J. Geophys. Res., Earth Surf. 121 (9), 1651–1675. https://doi.org/10.1002/2016JF003915.

Ganti, V., Chu, Z., Lamb, M.P., Nittrouer, J.A., Parker, G., 2014. Testing morphodynamic controls on the location and frequency of river avulsions on fans versus deltas: Huanghe (Yellow River), China. Geophys. Res. Lett. 41 (22), 7882–7890. https://doi.org/10.1002/2014GL061918.

Hajek, E.A., Wolinsky, M.A., 2012. Simplified process modeling of river avulsion and alluvial architecture: connecting models and field data. Sediment. Geol. 257, 1–30. https://doi.org/10.1016/j.sedgeo.2011.09.005.

Hoyal, D., Sheets, B., 2009. Morphodynamic evolution of experimental cohesive deltas. J. Geophys. Res., Earth Surf. 114 (F2). https://doi.org/10.1029/2007JF000882.

Jankowski, K.L., Törnqvist, T.E., Fernandes, A.M., 2017. Vulnerability of Louisiana's coastal wetlands to present-day rates of relative sea-level rise. Nat. Commun. 8, 14792. https://doi.org/10.1038/ncomms14792.

Jerolmack, D.J., 2009. Conceptual framework for assessing the response of delta channel networks to Holocene sea level rise. Quat. Sci. Rev. 28 (17), 1786–1800. https://doi.org/10.1016/j.quascirev.2009.02.015.

Jerolmack, D.J., Paola, C., 2007. Complexity in a cellular model of river avulsion. Geomorphology 91 (3), 259–270. https://doi.org/10.1016/j.geomorph.2007.04.022.

Kirwan, M.L., Temmerman, S., Skeehan, E.E., Guntenspergen, G.R., Fagherazzi, S., 2016. Overestimation of marsh vulnerability to sea level rise. Nat. Clim. Change 6 (3), 253–260. https://doi.org/10.1038/NCLIMATE2909.

Mohrig, D., Heller, P.L., Paola, C., Lyons, W.J., 2000. Interpreting avulsion process from ancient alluvial sequences: Guadalope-Matarranya system (northern Spain) and Wasatch Formation (western Colorado). Geol. Soc. Am. Bull. 112 (12), 1787–1803.

Moodie, A.J., Nittrouer, J.A., Ma, H., Carlson, B.N., Chadwick, A.J., Lamb, M.P., Parker, G., 2019. Modeling deltaic lobe-building cycles and channel avulsions for the Yellow River delta, China. J. Geophys. Res., Earth Surf. 124 (11), 2438–2462. https://doi.org/10.1029/2019JF005220.

Nienhuis, J.H., Ashton, A.D., Giosan, L., 2015. What makes a delta wave-dominated? Geology 43 (6), 511–514. https://doi.org/10.1130/G36518.1.

Nittrouer, J.A., Mohrig, D., Allison, M., 2011. Punctuated sand transport in the lowermost Mississippi River. J. Geophys. Res., Earth Surf. 116 (F4). https://doi.org/10.1029/2011JF002026.

Nittrouer, J.A., Shaw, J., Lamb, M.P., Mohrig, D., 2012. Spatial and temporal trends for water-flow velocity and bed-material sediment transport in the lower Mississippi River. GSA Bull. 124 (3–4), 400–414. https://doi.org/10.1130/b30497.1.

Paola, C., 2000. Quantitative models of sedimentary basin filling. Sedimentology 47 (s1), 121–178.

Paola, C., Twilley, R.R., Edmonds, D.A., Kim, W., Mohrig, D., Parker, G., et al., 2011. Natural processes in delta restoration: application to the Mississippi Delta. Annu. Rev. Mar. Sci. 3, 67–91. https://doi.org/10.1146/annurev-marine-120709-142856.

Peckham, S.D., Hutton, E.W., Norris, B., 2013. A component-based approach to integrated modeling in the geosciences: the design of CSDMS. Comput. Geosci. 53, 3–12. https://doi.org/10.1016/j.cageo.2012.04.002.

Pickering, J.L., Goodbred, S.L., Reitz, M.D., Hartzog, T.R., Mondal, D.R., Hossain, M.S., 2014. Late Quaternary sedimentary record and Holocene channel avulsions of the Jamuna and Old Brahmaputra River valleys in the upper Bengal delta plain. Geomorphology 227, 123–136.

Pizzuto, J.E., 1987. Sediment diffusion during overbank flows. Sedimentology 34 (2), 301–317.

Ratliff, K.M., Braswell, A.E., Marani, M., 2015. Spatial response of coastal marshes to increased atmospheric CO2. Proc. Natl. Acad. Sci. 112 (51), 15580–15584. https://doi.org/10.1073/pnas.1516286112.

Ratliff, K.M., Hutton, E.H.W., Murray, A.B., 2018. Exploring wave and sea-level rise effects on delta morphodynamics with a coupled river-ocean model. J. Geophys. Res., Earth Surf. 123 (11), 2887–2900. https://doi.org/10.1029/2018jf004757.

Shen, Z., Törnqvist, T.E., Mauz, B., Chamberlain, E.L., Nijhuis, A.G., Sandoval, L., 2015. Episodic overbank deposition as a dominant mechanism of floodplain and delta-plain aggradation. Geology 43 (10), 875–878. https://doi.org/10.1130/G36847.1.

Sincavage, R., Goodbred, S., Pickering, J., 2018. Holocene Brahmaputra River path selection and variable sediment bypass as indicators of fluctuating hydrologic and climate conditions in Sylhet Basin, Bangladesh. Basin Res. 30 (2), 302–320.

Sinha, R., 2009. The Great avulsion of Kosi on 18 August 2008. Curr. Sci. 97 (3), 429–433.

Slingerland, R., Smith, N.D., 2004. River avulsions and their deposits. Annu. Rev. Earth Planet. Sci. 32, 257–285. https://doi.org/10.1146/annurev.earth.32.101802.120201.

Syvitski, J.P., Kettner, A., 2011. Sediment flux and the Anthropocene. Philos. Trans. R. Soc. A, Math. Phys. Eng. Sci. 369 (1938), 957–975.

Syvitski, J.P.M., Kettner, A.J., Overeem, I., Hutton, E.W.H., Hannon, M.T., Brakenridge, G.R., et al., 2009. Sinking deltas due to human activities. Nat. Geosci. 2 (10), 681–686. https://doi.org/10.1038/ngeo629.

Syvitski, J.P.M., Overeem, I., Brakenridge, G.R., Hannon, M., 2012. Floods, floodplains, delta plains — a satellite imaging approach. Sediment. Geol. 267–268, 1–14. https://doi.org/10.1016/j.sedgeo.2012.05.014.

Tessler, Z.D., Vörösmarty, C.J., Grossberg, M., Gladkova, I., Aizenman, H., Syvitski, J.P.M., Foufoula-Georgiou, E., 2015. Profiling risk and sustainability in coastal deltas of the world. Science 349 (6248), 638. https://doi.org/10.1126/science.aab3574.

Törnqvist, T.E., Bridge, J.S., 2002. Spatial variation of overbank aggradation rate and its influence on avulsion frequency. Sedimentology 49 (5), 891–905.

van Toorenenburg, K., Donselaar, M., Noordijk, N., Weltje, G.J., 2016. On the origin of crevasse-splay amalgamation in the Huesca fluvial fan (Ebro Basin, Spain): implications for connectivity in low net-to-gross fluvial deposits. Sediment. Geol. 343, 156–164. https://doi.org/10.1016/j.sedgeo.2016.08.008.

Walling, D., He, Q., 1998. The spatial variability of overbank sedimentation on river floodplains. Geomorphology 24 (2), 209–223.

Wilson, C.A., Goodbred, S.L., 2015. Construction and maintenance of the Ganges-Brahmaputra-Meghna delta: linking process, morphology, and stratigraphy. Annu. Rev. Mar. Sci. 7 (1), 67–88. https://doi.org/10.1146/annurev-marine-010213-135032.